Sensors and Actuators A 196 (2013) 22–29

Contents lists available at SciVerse ScienceDirect

Sensors and Actuators A: Physical

journal homepage: www.elsevier.com/locate/sna

A monolithic poly(dimethylsiloxane) electrostatic actuator for controlling integrated pneumatic microsystems

Joshua D. Tice[a], Thomas A. Bassett[a], Amit V. Desai[a], Christopher A. Apblett[b,c], Paul J.A. Kenis[a,*]

[a] Department of Chemical & Biomolecular Engineering, University of Illinois at Urbana-Champaign, Urbana, IL 61801, USA
[b] Sandia National Laboratories, Albuquerque, NM 87185, USA
[c] Department of Chemical & Nuclear Engineering, University of New Mexico, Albuquerque, NM 87131, USA

ARTICLE INFO

Article history:
Received 7 December 2012
Received in revised form 16 February 2013
Accepted 15 March 2013
Available online 23 March 2013

Keywords:
Electrostatic actuator
Microvalve
Microfluidics
Soft-lithography
Pneumatic microsystems

ABSTRACT

Although pneumatic microvalves are widely utilized in microfluidic systems, they are rarely used in portable applications due to the bulky ancillary equipment required for their actuation. The microvalves rely on transducers that convert electrical signals into mechanical forces, and the miniaturization and integration of these transducers has proven to be challenging. Here, we report a strategy for operating pneumatic valves where microscale electrostatic actuators were used to relay commands from electronic ancillaries. Each electrostatic actuator occupied a footprint less than 0.5 mm^2, and was composed entirely of poly(dimethylsiloxane) and multi-walled carbon nanotubes. Similar to typical pneumatic microvalves, the electrostatic actuators were fabricated exclusively with soft-lithographic techniques, which permitted both components to be integrated monolithically. The actuators operated at electric potentials less than 300 V, and regulated microchannels pressurized up to ~4 kPa, which is sufficient for many microfluidic applications.

1. Introduction

Pneumatic microvalves have been widely implemented in chemical and biological microsystems (*e.g.*, platforms for protein crystallization screening [1,2], genomic analysis [3], and biological network characterization [4]) due to their unique combination of simplicity, reliability, and versatility [5]. However, despite their many advantages, pneumatic microvalves have one major drawback. They are typically operated with an external pressure source, an array of solenoid valves, and computerized controls, which severely limit their portability. A common strategy that has emerged to address this issue involves the compression of microfluidic reservoirs either with (i) battery-operated arrays of solenoids [6] or (ii) refreshable Braille displays [7]. In practice, this approach is limited to systems with densities on the order of ~10 pneumatic microvalves per cm^2, since solenoids scale at ~1 actuator per cm^2, and Braille displays scale at ~10 actuators per cm^2. Additionally, neither actuator has been shown to operate more than several valves per control channel due to the attenuation of pressure pulses. Consequently, both solenoids and Braille displays will meet challenges when applied to highly-parallelized, microfluidic large scale integrated systems, where pneumatic microvalves are routinely fabricated with densities on the order of 1000 valves per cm^2 [8], and recent examples achieve densities approaching 10^6 valves per cm^2 [9].

A second strategy for controlling portable pneumatic microsystems utilizes electrostatic microvalves that gate pneumatic control lines pressurized with an external gas tank [10]. Due to the low dead volume of the electrostatic microvalves, the pressure source can be scaled down to a portable size. Although this approach is also limited to densities of ~10 actuators per cm^2, the pressure from the tank can hypothetically drive hundreds of valves per control line. Unfortunately, dielectric charging rapidly increases the actuation potentials during cycling, and eventually renders the valves inoperable. Also, fabrication of the electrostatic actuators is tedious, and interfacing with the microfluidic chip requires multiple pneumatic connections.

Herein, we report ancillary electrostatic actuators that scale appropriately for large scale integrated microfluidic systems (~100 actuators per cm^2). The actuators were fabricated exclusively with simple soft-lithographic techniques, which allowed them to be easily incorporated into standard pneumatic microsystems without the need for sophisticated microfabrication equipment. Also, drift in the actuation potential due to dielectric charging was avoided by fabricating contact surfaces from identical materials.

* Corresponding author at: 600 South Mathews Avenue, Urbana, IL 61801, USA. Tel.: +1 217 265 0523; fax: +1 217 333 5052.
E-mail address: kenis@illinois.edu (P.J.A. Kenis).

0924-4247/$ – see front matter © 2013 Elsevier B.V. All rights reserved.
http://dx.doi.org/10.1016/j.sna.2013.03.020

2. Design

The design of our electrostatic actuator is shown in Fig. 1. Each actuator consisted of a circular elastomeric membrane with an embedded electrode, suspended above a microfluidic chamber. In the application we explore here, this chamber was part of the control channel leading to one or more pneumatic microvalves. A second electrode was embedded just beneath the floor of the chamber. A cylindrical post was attached to the top of the membrane to both reduce the probability of adhesion-driven collapse [11–13] and reduce upward deflection of the membrane when the channel was pressurized. The recess above the membrane was connected to a channel that was vented to atmosphere to avoid pressure build-up in the cavity, which could affect actuation. Based on a mathematical model we developed earlier [11], we designed the diameter of the membrane to be between 200 and 600 μm, which permitted actuation at low potentials (<300 V) while avoiding collapse due to adhesion between the membrane and the chamber floor. The diameters reported here were significantly smaller than those of previously reported electrostatic actuators for instructing pneumatic microvalves (3 mm) [10]. With these lateral dimensions, we anticipate our actuators will scale on the order of ~100 actuators per cm^2, an order of magnitude higher than previously reported transducers.

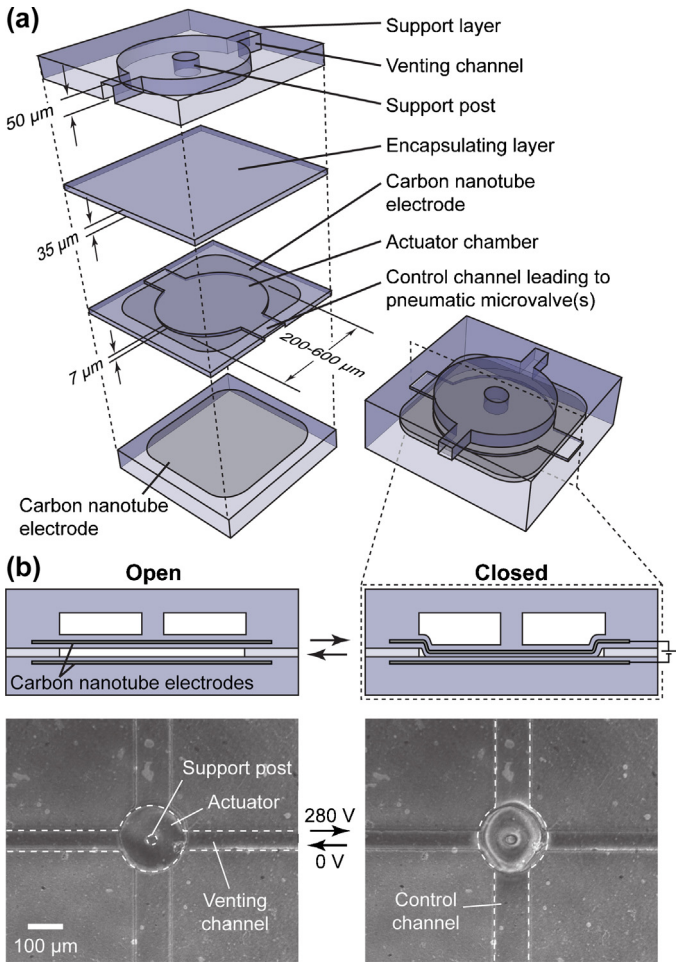

Fig. 1. (a) An exploded view and a perspective view of the monolithic poly(dimethylsiloxane) electrostatic actuator. Vertical dimensions are not drawn to scale. (b) Side views (illustrations) and top views (micrographs) of electrostatic actuators in the open and closed states. In the micrographs, the carbon nanotube electrodes extend beyond the view of the images.

3. Materials and methods

3.1. Fabrication

Molds for channels and actuator chambers were made by patterning SU-8 5 photoresist (Microchem Corp., Newton, MA) onto silicon wafers using standard photolithographic techniques in accordance with the manufacturer's specifications. The photoresist was spun at 1700 rpm for 30 s, leading to features 7 μm tall. Molds for the stamps and support layer were fabricated using SU-8 50 spun at 2000 rpm for 30 s, resulting in features 50 μm tall. To reduce adhesion between poly(dimethlysiloxane) (PDMS) and the molds, a surface treatment was performed by placing the molds in a vacuum desiccator along with several drops of (tridecafluoro-1,1,2,2-tetrahydrooctyl)trichlorosilane (Gelest, Inc., Morrisville, PA), and then applying vacuum overnight.

To form the electrodes, an aqueous suspension of multi-walled carbon nanotubes (MWNTs) (20–30 nm outer diameter, 10–30 μm length, >95 wt% purity, ash <1.5 wt%; Cheaptubes, Inc., Brattleboro, VT) with a ratio of 1 g MWNTs: 10 g sodium dodecyl sulfate: 1 mL deionized water was prepared and sonicated (Vibra-Cell VCX130PB; Sonics & Materials, Inc., Newtown, CT) for approximately 30 min to solubilize the MWNTs. A 0.1 mL sample was diluted into approximately 20–30 mL deionized water and stirred briefly. The dilute suspension was filtered through an alumina membrane (Whatman Anodisc™ inorganic membrane, 0.1 or 0.2 μm pore size, 47 mm diameter) that had been wet with ethanol (Fig. 2a) [14]. After the liquid had fully passed through the membrane, the MWNTs that remained on the membrane were washed with ethanol until the filtrate was free of bubbles.

To construct the upper layers of the actuator, a thin layer of PDMS (20:1 ratio of monomer to cross-linking agent by weight; General Electric RTV 615; Hisco, Inc., Schaumburg, IL) was first spin-coated onto the mold at 10,000 rpm for 50 s such that a thin film (~8 μm thick) covered the channel features (Fig. 2b). The PDMS film was cured in an oven at 70 °C for 1 h and then allowed to cool to room temperature. A PDMS stamp (20:1 ratio of monomer to cross-linking agent by weight, cured overnight at 70 °C) was brought into contact with the MWNT film formed previously. Areas in contact with the stamp were lifted off the membrane filter and then applied to the PDMS film [15]. Pressure was applied by hand, and then the stamp was removed. Electrical contacts were made from a mixture of PDMS (5:1 ratio of monomer to cross-linking agent by weight) and 10 wt% MWNTs, which was applied on the designated area of the MWNT electrode and subsequently cured for 15 min in an oven at 70 °C. To encapsulate the MWNT electrode, a second layer of PDMS (20:1 ratio of monomer to cross-linking agent by weight) was spin-coated on top of the electrode at 2400 rpm for 30 s (~35 μm thick) and allowed to cure until tacky in an oven at 70 °C for 20–30 min. The PDMS support layer (5:1 ratio of monomer to cross-linking agent by weight; cured at 70 °C for 1 h) was aligned and placed on the membrane. The support layer contained cylindrical posts centered in the recesses over the actuator chambers that were 20% the diameter of the underlying chambers. After aligning the support layer, uncovered regions of the spin-coated PDMS layers were filled with liquid PDMS (5:1 ratio of monomer to cross-linking agent by weight) and the whole assembly was cured overnight in an oven at 70 °C. Afterward, the upper layers of the actuator were removed from the mold and holes were punched to the inlets of the microchannels using a sharpened 20 gauge steel needle.

To fabricate the lower electrode for the actuator, a featureless silicon wafer was treated with silane vapor as described previously, and a thin layer of PDMS (20:1 ratio of monomer to cross-linking agent by weight), diluted in hexanes (10:1 ratio of hexanes to PDMS by weight) was spin-coated onto the wafer at 10,000 rpm for 120 s,

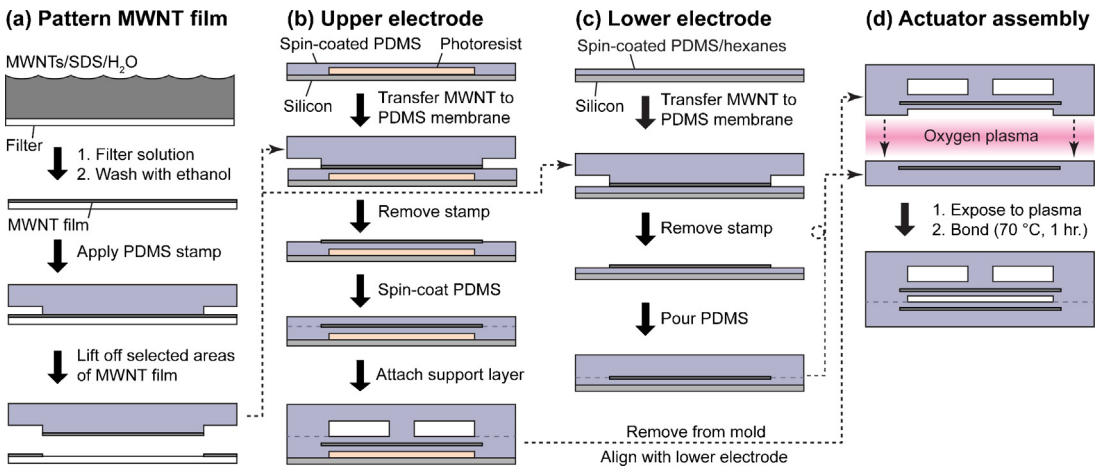

Fig. 2. An illustration of the fabrication scheme for monolithic electrostatic actuators using soft-lithographic techniques.

yielding a film <1 μm thick (Fig. 2c) [16]. The thin PDMS layer was cured in an oven at 70 °C for 1 h, and then a MWNT film was deposited as described above. Electrical contacts were also applied, and the wafer was then covered with a layer of PDMS (5:1 ratio of monomer to cross-linking agent by weight) several millimeters thick. The PDMS was cured overnight at 70 °C.

To seal the upper layers of the actuator to the lower electrode, both surfaces participating in the seal were exposed to oxygen plasma generated with an atmospheric plasma system (Atomflo™ 400L system equipped with an AH-250L head; Surfx Technologies, Redondo Beach, CA) (Fig. 2d). The system was configured to 100 W RF power, with an oxygen flow rate of 0.03 L min^{-1} and a helium flow rate of 15.0 L min^{-1}. The bonding surfaces were passed under the nozzle of the plasma system by hand at approximately 2 cm s^{-1}. Immediately after exposure, the separate layers were aligned and brought into contact. To complete the seal, the device was heated at 70 °C for at least 1 h.

3.2. Determination of actuator dimensions

To determine critical dimensions, an actuator was cut in half to expose the cross-section and then observed with a scanning electron microscope (JEOL 6060LV SEM). Channel depths were measured with a profilometer (Dektak 3030). Lateral dimensions were measured with an optical stereoscope (Leica M025C).

3.3. Integration of electrostatic actuators with a pneumatic microvalve

To integrate a pneumatic microvalve into the device, the fabrication of the lower electrode was modified as follows. After spin-coating PDMS, depositing the electrode, and curing the electrical contacts, a second layer of PDMS (20:1 ratio of monomer to cross-linking agent by weight) was spin-coated onto the wafer at 2400 rpm for 30 s (~35 μm thick). The PDMS layer was semi-cured in an oven at 70 °C for 20–30 min, until tacky. The reagent channel for the pneumatic valve was placed on top. Uncovered regions of the spin-coated PDMS layers were filled with liquid PDMS (5:1 ratio of monomer to cross-linking agent by weight) and the whole assembly was cured overnight at 70 °C. The mold for the reagent channel was made by spin-coating Microposit™ SPR220™-7 photoresist at 1500 rpm for 60 s (10 μm thick). The remainder of the photoresist processing was performed according to the manufacturer's specifications. Following development, the mold was heated at 150 °C for 30 min to allow the resist to reflow, which created a rounded cross-section. The rounded cross-section permitted hermetic closure of the pneumatic microvalve [17].

3.4. Characterization of the transfer printing process

Films of MWNTs were formed with solution-based processes as described in Section 3.1. Sheet resistance was measured with a custom-made four point probe while the films were still on the membrane filters. The films were then transferred to featureless PDMS stamps (20:1 ratio of monomer to cross-linking agent by weight, cured at 70 °C overnight) without leaving observable residue on the filtration membranes. The optical absorbance of MWNT films with known densities were measured with a Perkin Elmer Lambda 650 UV/Vis spectrometer at a wavelength of 400 nm (while still on the PDMS stamps) to produce a calibration curve of optical absorbance relative to nanotube density. Then, MWNT films (initially 40 μg cm^{-2}) were transferred from stamps to PDMS membranes, and then encapsulated with another layer of PDMS. The calibration curve was then used to extrapolate the final densities of the MWNT films.

3.5. Characterization of drift in the actuation potential

The actuator chambers were filled with fluorinated oil (3M™ Fluorinert™ FC-40), wires were inserted into the electrical contacts on the device, and the wires were attached to electrical leads connected to a DC power supply (Hewlett Packard model 6209B). The electrode embedded in the membrane was negatively polarized. The potential was increased slowly (~10 V s^{-1}) until the membrane came into contact with the floor of the actuator chamber. Afterward, the potential was released, and the process was repeated immediately afterward. The actuator was viewed under an inverted microscope (Leica, DMI4000) equipped with a 1600 × 1200 pixel charge-coupled device camera (QImaging, Retiga-2000R) and phase contrast optics to visualize contact of the membrane with the floor of the actuator chamber.

3.6. Testing electrostatic gates coupled to a pneumatic microvalve

The electrodes were interfaced with the power source as reported in the previous section. The inlet of the control channel was attached to a vial filled with fluorinated oil (3M™ Fluorinert™ FC-40) and attached to a source of pressurized nitrogen *via* a pressure controller (Cole Parmer, model 68027-780). The inlet pressure was adjusted to 8 kPa, and the outlet was vented to atmosphere. The reagent channel was filled with a mixture of

blue dye (for optical contrast) with 50% ethanol by volume. To shut the pneumatic microvalve, a potential of 300 V was applied to the gate downstream of the pneumatic microvalve. To open the pneumatic microvalve, the same potential was applied to the upstream gate, and then the potential applied to the downstream gate was released. Images were captured through a stereoscope (Leica M025C). To measure the leakage rate of the hydraulic fluid, a ~10 mm length of 30 gaugeTeflon® tubing was attached to the outlet, and one of the gates was closed with a potential of 300 V. Hydraulic fluid was collected in the tubing over the course of 5 min. The volume of the collected fluid was then calculated using the length of the fluid slug and the inner diameter of the tubing. Dividing by the duration of fluid collection yielded the flow rate.

3.7. Characterization of pressures accommodated by the electrostatic actuator

The actuator chambers were filled with fluorinated oil (3M™ Fluorinert™ FC-40), and the device was attached to the power source as mentioned previously. The inlet of the control channel was attached to a source of pressurized nitrogen *via* a pressure controller (Cole Parmer, model 68027-780). The outlet was shut with a piece of Teflon® tubing that was filled with cured PDMS. A potential was applied across the electrodes to close the gate, and then the pressure in the gate chamber was increased slowly (~0.1 kPa s^{-1}) until the membrane released from the floor of the microchannel. Afterward, the pressure was decreased at the same rate until the membrane snapped back into contact with the channel floor. This process was repeated at least three times per gate.

4. Results and discussion

4.1. Advantages of carbon nanotube electrodes

As mentioned previously, one of the main objectives of our work was to develop a simple fabrication scheme for the electrostatic actuator, which required a careful evaluation of the materials used for the electrodes. Others have mainly formed electrodes made from thin metallic films [10,18–24]. However, to deposit metallic films, fabrication procedures such as high-vacuum deposition, aggressive chemical etching, and/or high-temperature annealing steps are required. We sought to utilize fabrication techniques that were less intensive, inexpensive, and minimally hazardous. Metal electrodes also have a propensity to buckle when deposited on elastomers [25], and in certain instances, the thin films require specially-tailored channel cross-sections to prevent them from fracturing under strain [24,26].

To address the above issues, we formed electrodes from conducting nanoparticles. Specifically, we used multi-walled carbon nanotubes, because several highly effective solution-based methods have been reported for depositing and patterning films of the nanoparticles [14,15]. Since carbon nanotubes are hydrophobic, they adhered well to PDMS stamps and could be patterned and deposited *via* microtransfer printing, with 37% ± 17 (SD) of the electrode material transferring from the stamp to the substrate (Fig. 3a).

Several other characteristics of carbon nanotubes made them an attractive choice for electrodes. Due to the high aspect ratios of carbon nanotubes (*i.e.*, ratios of length to width), the nanoparticles form fully percolating networks at lower loadings than globular nanoparticles (*e.g.*, carbon black) [27]. The particle loading was adjusted such that the electrodes were both conductive and transparent, which aided in visualizing the flow of fluids through the actuators [14,28,29]. For the particle loadings we used, the average optical absorbance was 0.3, and the sheet resistance was ~1.5 kΩ sq^{-1} (Fig. 3b). Finally, carbon nanotube-polymer composites have been shown to withstand high stresses without mechanical failure [30–32], and multi-walled carbon nanotubes can be procured easily from commercial sources.

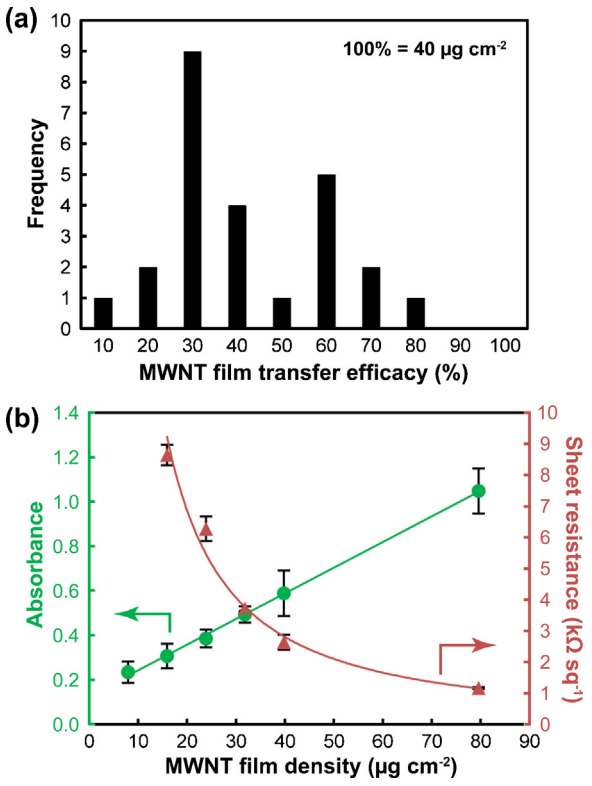

Fig. 3. Characterization of electrodes made from multi-walled carbon nanotubes. (a) A histogram showing the extent of MWNT transfer from PDMS stamps to PDMS substrates in a sample of 25 devices, as determined by optical absorbance at 400 nm. The MWNT films had initial loading of 40 μg cm^{-2} before transfer. (b) Quantification of film transparency and sheet resistance as a function of MWNT loading. Error bars represent one standard deviation.

4.2. Characterization of actuation potentials

We characterized the minimum electric potential needed to close the actuator, initially with atmospheric pressure applied to the control channel. We tested three different diameters (200, 400, and 600 μm). For each actuator, the total thickness of the membrane was 35 ± 6 μm; the channel was 7 μm high; and the support post was 20% of the diameter of the membrane. The width and height of the venting channel in the support layer were both 50 μm. The control channel leading to the actuator was 100 μm wide and 7 μm tall. The thickness of the MWNT electrodes was ~1 μm.

The actuator chamber was filled with hydraulic fluid (3M™ Fluorinert™ FC-40), which served to reduce the actuation potential (due to its higher dielectric constant relative to air) and to reduce the probability of adhesion-driven collapse [11]. An electric potential was gradually applied across the electrodes, increasing at a rate of ~10 V s^{-1}. The membrane deflected slowly until it reached a threshold where it suddenly snapped shut against the lower electrode, which we refer to as the actuation potential (Fig. 1b). Actuators with 200 μm diameters actuated at 233 ± 19 V (SD); actuators with 400 μm diameters actuated at 157 ± 18 V (SD); and actuators with 600 μm diameters actuated at 113 ± 20 V (SD). With 280 V applied, approximately 80% of the valve seat was in contact with the membrane, as measured through optical microscopy with phase contrast optics.

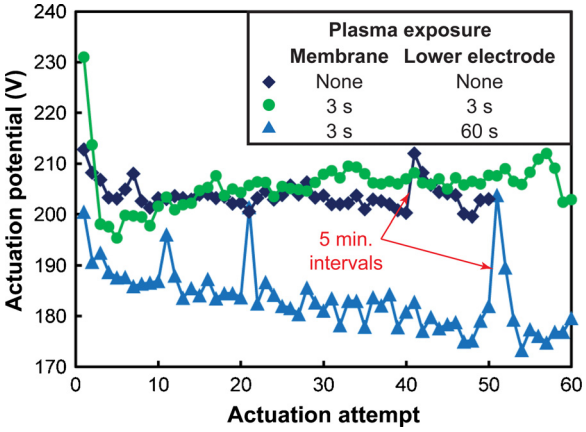

Fig. 4. Actuation potential as a function of number of actuation attempts for actuators assembled with three different surface treatments. The duration between actuation attempts was less than 1 min, except where indicated by red arrows. (For interpretation of the references to color in this figure legend, the reader is referred to the web version of this article.)

4.3. Minimizing drift in the actuation potential by ensuring material symmetry

Continuously cycling a contact-mode electrostatic actuator often causes a shift in the actuation potential, which eventually renders the actuator inoperable [10,33–35]. The shift has been attributed to contact electrification (*i.e.*, the triboelectric effect), which arises from chemical differences between the two surfaces coming into contact [36]. We observed this phenomenon with a previously reported electrostatic actuator, where the membrane was constructed from PDMS, and the lower electrode was composed of an indium tin oxide film on glass [11]. By applying identical chemical treatments to the surfaces, others have been able to minimize the drift in potential [34–37]. Hence, we hypothesized that the potential drift could be minimized by fabricating the membrane and the floor of the actuator chamber from the same elastomer. To keep surface modifications identical, both the membrane and the channel floor were exposed to oxygen plasma for the same time (~3 s exposure each) during the final step of the fabrication process (Fig. 2d).

We cycled an actuator with a diameter of 200 μm, with all other dimensions the same as those listed in Section 4.2. Less than 1 min was allowed to elapse between actuation events (except in given instances mentioned below). We observed that during the first several cycles, the actuation potential decreased rapidly at a rate of ~10 V per actuation event (Fig. 4). Afterward, the actuation potential increased gradually (≤1 V per actuation) until it reached a plateau and stabilized after ~35 cycles. Our design improves over previously reported actuators, where actuation potentials drifted 20–30 V per cycle without stabilizing [10].

With our current atmospheric plasma system, the speed at which the substrate passed under the nozzle of the plasma could not be controlled precisely. Hence, we hypothesized that the transient drift in potential observed in the above experiment could have been partly due to inadvertent variations in exposure time. To investigate our hypothesis, we purposefully treated the bonding surfaces with different lengths of plasma exposure. The membrane side of the actuator was exposed to plasma for ~3 s, and the opposing side was exposed for ~1 min. When the actuator was cycled, the potential dropped ~10 V during the first two actuation events, and then continued to decrease at a rate of ~0.4 V per actuation for the remainder of the test (Fig. 4). In contrast, when neither side of the actuator was exposed to plasma during assembly, no sustained drift in the actuation potential was observed. The potential stabilized immediately after dropping ~10 V during the first four cycles. Without plasma treatment, however, the two sides of the actuator did not seal permanently. We predict that if the plasma treatment of the bonding surfaces could be controlled more precisely, the actuator would still operate with negligible drift in actuation potential, and a permanent bond could be formed as well.

Several other observations are worthy of mention. Irrespective of plasma treatment, a sharp drop in actuation potential occurred at the beginning of all the cycling tests. This could possibly be due to charge injection or the rearrangement of the MWNT network following strain of the membrane. Also, the actuation potential was sensitive to the frequency of actuation. When 5 min were allowed to elapse between actuation events instead of ~1 min (Fig. 4), the actuation potential shifted to its initial value from the beginning of the cycling test. Upon increasing the frequency, the actuation potential dropped sharply again until it recovered its value prior to the 5 min pause. The mechanism behind this phenomenon is unclear at this time, but one hypothesis is that lower frequencies could have allowed time for PDMS oligomers to migrate to the surface where they could displace charged chemical moieties [38].

4.4. Controlling pneumatic microvalves with electrostatic actuators

The design of the electrostatic actuator permitted simple, monolithic integration with pneumatic microsystems. Our strategy for relaying instructions to pneumatic microvalves with the electrostatic actuators is shown in Fig. 5. The pneumatic microvalve was driven by hydraulic fluid (3M™ Fluorinert™ FC-40) that was pressurized with a cylinder of compressed nitrogen. Using hydraulic fluid in the place of air prevents air from migrating out of the control channel, through the gas-permeable PDMS membrane of the pneumatic valve, and into the reagent channel. A reservoir of the hydraulic fluid was attached to the inlet of the microvalve's control channel. The outlet of the control channel was vented to atmosphere. Two electrostatic actuators were integrated into the control channel, which had a width of 50 μm, a height of 7 μm, and a length of 14 mm. One actuator was placed upstream and the other was placed downstream of the pneumatic microvalve. The actuators worked against the pressure from the tank (8 kPa), serving to block fluid flow in the control channel and switch between the external source and atmosphere. Hence, we refer to the actuators as "gates".

When the upstream gate was closed with a potential of 300 V and the downstream gate was left open, the control channel was vented to atmosphere, and the pneumatic microvalve remained open (Fig. 5a and c). When the upstream gate was opened and the downstream gate was closed, pressurized hydraulic fluid filled the control channel, which closed the pneumatic microvalve (Fig. 5b and d). The rounded cross-section of the reagent channel led to hermetic seal [5,17]. In contrast, the cross-sectional profile of the chamber of the electrostatic actuator was rectangular, which prevented the periphery of the membrane from shutting completely (see Fig. 1b) [23], which resulted in fluid leakage through the control channel during operation. However, the fluidic resistance of the control channel was high enough to result in low leakage rates, on the order of microliters per week.

In this proof-of-principle demonstration, only one pneumatic microvalve was controlled by two electrostatic gates. However, hypothetically two gates could control tens or even hundreds of valves in parallel [8].

4.5. Characterization of operating pressures

The back pressure that an electrostatic gate could accommodate was limited by one of two thresholds: (i) the maximum pressure

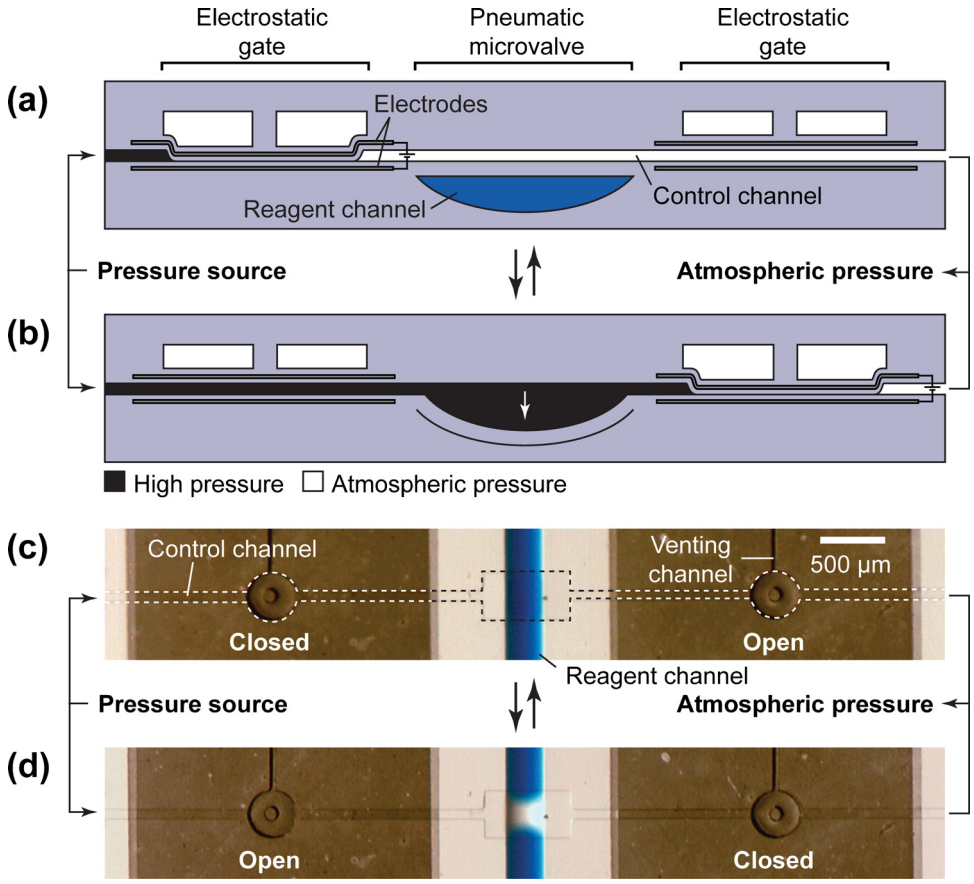

Fig. 5. (a) and (b) Illustrations (side view) and (c) and (d) micrographs (top view) of a pneumatic microvalve controlled with two electrostatic gates. In the control channel in (a) and (b), black-colored regions denote high pressure, while white-colored regions denote atmospheric pressure. In (c) and (d), the device was illuminated at an angle to provide sufficient contrast to visualize the channel edges. This illumination scheme also resulted in an optical gradient that affected rounded features, in particular the reagent channel. In (d), the dark region on the left side of the pneumatic microvalve is due to this optical effect, and not the presence of blue dye. (For interpretation of the references to color in this figure legend, the reader is referred to the web version of this article.)

that could be applied to the control channel while still permitting the electrostatic gate to close, or (ii) the maximum pressure that the electrostatic gate could isolate in its closed state before being forced open.

We quantified both these thresholds. With the pressure of the control channel high enough to keep the gate opened, we applied a constant potential and then slowly decreased the pressure until the gate snapped shut. Then, we increased the pressure until the gate re-opened (Fig. 6).

In the scenario where gates were initially open, the pressure that could be applied while still permitting actuation increased linearly relative to electric potential (Fig. 6a). Using a gate with a diameter of 400 μm and a potential of 280 V, up to 4 kPa of pressure could be applied to the control channel while still allowing the actuator to shut.

The effect of actuator diameter appeared to be insignificant. To explain this latter trend, we refer to a model based on the theory of parallel plate capacitors [11]. The pressure exerted on the membrane due to an applied potential (p_{elec}) is given by the following expression, assuming the actuator is in the open state (Fig. 7a):

$$p_{elec} = \frac{1}{2}\frac{\varepsilon_0 \varepsilon_{fluid} V_{app}^2}{((h_c/\varepsilon_m) + g)^2} \quad (1)$$

where ε_0 is the permittivity of free space, ε_{fluid} the relative permittivity of the fluid, V_{app} the applied electric potential, h_c the thickness of the insulating layer beneath the conducting layer of the top electrode, ε_m the relative permittivity of the membrane material, and g the gap between the electrodes.

In this scenario, the pressure generated by the electric potential is a function of the gap, not the geometrical configuration (*e.g.*, shape or diameter) of the membrane.

When the gates were initially shut, the pressures that could be isolated also appeared to increase linearly with electric potential. The highest pressure isolated was 30 kPa, using a gate with a diameter of 200 μm and an applied potential of 280 V.

Gates with smaller diameters were more effective at isolating pressure in the control line before re-opening. The reason for this diameter dependence is that the pressure required to detach the membrane is a function of the stored potential energy in the deformed membrane, which in turn depends on diameter. Consider the diagram in Fig. 7b. To estimate the pressure required to reopen the gate from the closed state, we first estimate the pressure required to reopen the gate (p_{det}) when no potential is applied. We estimate the pressure needed to collapse a membrane ($p_{collapse}$) with a radius of collapse, b, by balancing the potential energy stored in the membrane and the energy due to pressure (see Eq. (60) from [39]). The expression for p_{det} is derived as follows:

$$p_{collapse} = \frac{64 D K_{bilayer} K_{MS}}{K_{AR} a^4}\left[\frac{1}{3(1-\beta^4) + 8\beta^2 \log \beta}\right]$$

$$D = \frac{Et^3}{12(1-\nu^2)}; \quad \beta = \frac{b}{a} \quad (2)$$

where E is the Young's modulus of the membrane material, t the total thickness of the membrane, ν the Poisson's ratio of the membrane material, a, b defined in Fig. 7, $K_{bilayer}$ the factor to account

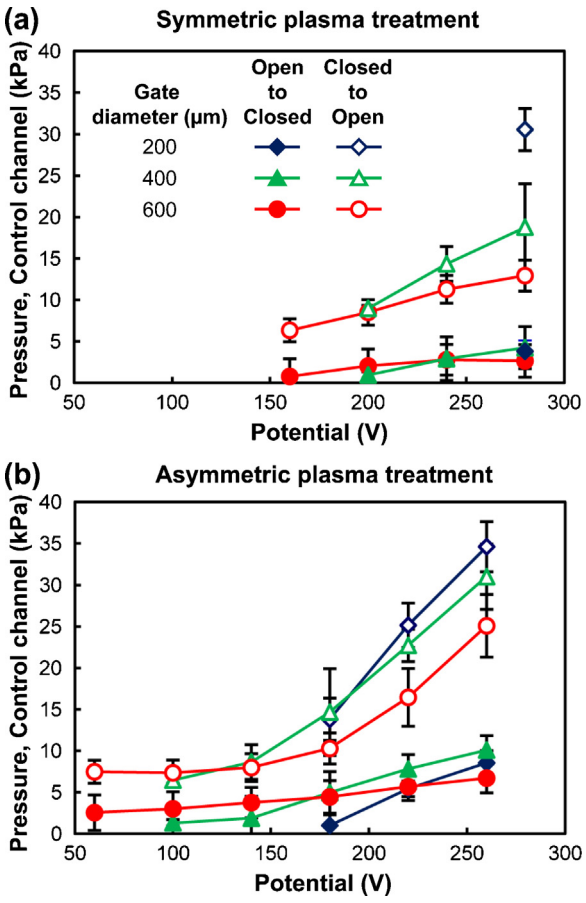

Fig. 6. Graphs of the potentials needed to close electrostatic gates as a function of the pressure in the control channel (solid symbols), and the pressures needed in the control channel to re-open the gates at fixed potentials (open symbols). Two scenarios are shown: (a) for gates that were sealed with a symmetric plasma treatment (~3 s exposure for each bonding surface), and (b) those sealed with an asymmetric treatment (~3 s exposure for the membrane, and ~60 s exposure for the lower electrode). A minimum of three gates were tested for each data point. Error bars represent one standard deviation.

for a bilayer configuration where the electrode is embedded within the membrane; the expression for this factor has been derived elsewhere [11], K_{MS} the factor to account for membrane stresses (MS) and is given by

$$K_{MS} = 1 + 0.488\left(\frac{g}{t}\right)^2 \quad [39]$$

K_{AR} is the factor to account for aspect ratio (AR) and is given by

$$K_{AR} = 1 + \frac{16}{1-\nu}\left(\frac{t}{D}\right)^2 \quad [39]$$

The valve will spontaneously detach when $\beta = 0.175$, which is based on instability in the system [40]. Therefore, p_{det} is given by

$$p_{det} = \frac{64DK_{bilayer}K_{MS}}{K_{AR}a^4}\left[\frac{1}{2.57}\right] \quad (3)$$

In presence of an applied potential, the total pressure required to reopen a valve is given by

$$p_{reopen} = p_{det} + p_{elec} \quad (4)$$

Although p_{elec} is independent of diameter, p_{det} is not, which results in the observed dependence of the pressure required to reopen the valve on membrane diameter.

For the data shown in Fig. 6a, the electrostatic gates were assembled by treating both halves with ~3 s of plasma exposure during fabrication. By increasing the plasma exposure to the lower electrode during fabrication (~1 min), thereby inducing dielectric charging and greater attraction between the membrane and the channel floor, we increased the operating pressures of the gates (Fig. 6b). Before quantifying the threshold pressures, we conditioned the gates by actuating them 50 times each.

The non-linear trend between actuation potential and pressure, predicted by Eqs. (1) and (4), became more pronounced under these conditions. The highest pressure that could be applied to the control channel while still allowing the gate to actuate was 10 kPa. The maximum pressure isolated by a gate in the closed state was 35 kPa. If the actuators were conditioned for more cycles, the operating pressures would likely have increased further. However, eventually drift in the actuation potential would likely cause the membrane to adhere permanently to the chamber floor. For situations where less than one hundred actuation cycles are needed, this strategy might find utility. For other scenarios, we are exploring different means of increasing operating pressures, *e.g.*, by balancing the pressure above and below the membrane [37,41].

Currently, controlling pneumatic actuators with the electrostatic gates will be limited by the maximum operating pressure when the gate is initially open, which is 4 kPa for gates that have been treated symmetrically with plasma. Pressures of this magnitude are adequate to operate pneumatic valves in a wide range of microfluidic applications [17].

5. Conclusions

In summary, we developed a monolithic electrostatic actuator made completely from PDMS and MWNTs that scales at a rate of ~100 actuators per cm^2. By ensuring material symmetry between the membrane and the channel floor, we were able to reduce drift in the actuation potential. Also, since the actuator was fabricated exclusively with soft-lithographic techniques, we were able to integrate the actuator with standard pneumatic microvalves in a straight-forward manner. Currently, the electrostatic actuators (or gates) can accommodate pressures up to ~4 kPa. However, by introducing a material asymmetry between the membrane and the seat of the actuators, the actuators were able to accommodate pressures up to ~10 kPa (although this reintroduces the issue of

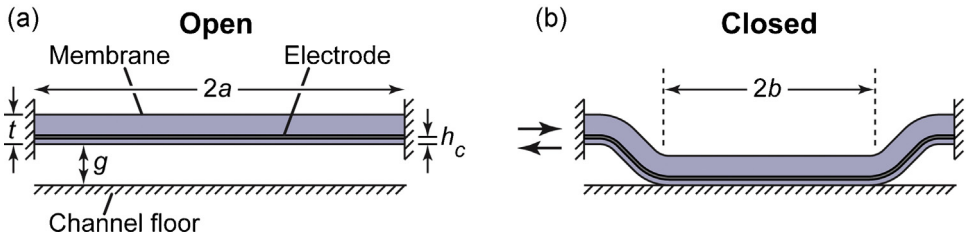

Fig. 7. Simplified illustration of the cross-section of an electrostatic actuator in the (a) open and (b) closed states. Relevant geometrical parameters are indicated.

drift in the actuation potential over time). In their current form, the electrostatic actuators require only a small pressure source and a power source to operate. We predict that improvements to the electronics used to the control the actuators will result in fully portable pneumatic microsystems, which will lead to sophisticated platforms for mobile chemical detection or point-of-care diagnostics.

Acknowledgements

We thank Dr. Gregory Ten Eyck, Andrew Collard, and Christopher Hamlin for performing preliminary fabrication and characterization. Dane Sievers assisted in measuring the sheet resistance of the carbon nanotube electrodes. Dr. James Wentz provided electrical testing equipment. We also gratefully acknowledge financial support from Sandia National Laboratories, funded by the DOE through grant LDRD PR#922327; the Center for Nanoscale Chemical Electrical Mechanical Manufacturing Systems at the University of Illinois, funded by the NSF through grant DMI-0328162; and the Center for Microanalysis of Materials in the Frederick Seitz Materials Research Laboratory Central Facilities at the University of Illinois.

References

[1] M.J. Anderson, C.L. Hansen, S.R. Quake, The use of microfluidic devices towards protein crystallography, Biophysical Journal 88 (2005) 55A.
[2] S.L. Perry, G.W. Roberts, J.D. Tice, R.B. Gennis, P.J.A. Kenis, Microfluidic generation of lipidic mesophases for membrane protein crystallization, Crystal Growth & Design 9 (2009) 2566–2569.
[3] M. Diehn, R.W. Cho, N.A. Lobo, T. Kalisky, M.J. Dorie, A.N. Kulp, D.L. Qian, J.S. Lam, L.E. Ailles, M.Z. Wong, B. Joshua, M.J. Kaplan, I. Wapnir, F.M. Dirbas, G. Somlo, C. Garberoglio, B. Paz, J. Shen, S.K. Lau, S.R. Quake, J.M. Brown, I.L. Weissman, M.F. Clarke, Association of reactive oxygen species levels and radioresistance in cancer stem cells, Nature 458 (2009), 780-U123.
[4] P.M. Fordyce, D. Gerber, D. Tran, J. Zheng, H. Li, J.L. DeRisi, S.R. Quake, De novo identification and biophysical characterization of transcription-factor binding sites with microfluidic affinity analysis, Nature Biotechnology 28 (2010) 970–975.
[5] M.A. Unger, H.P. Chou, T. Thorsen, A. Scherer, S.R. Quake, Monolithic microfabricated valves and pumps by multilayer soft lithography, Science 288 (2000) 113–116.
[6] K.A. Addae-Mensah, Y.K. Cheung, V. Fekete, M.S. Rendely, S.K. Sia, Actuation of elastomeric microvalves in point-of-care settings using handheld, battery-powered instrumentation, Lab on a Chip 10 (2010) 1618–1622.
[7] W. Gu, H. Chen, Y.-C. Tung, J.-C. Meiners, S. Takayama, Multiplexed hydraulic valve actuation using ionic liquid filled soft channels and braille displays, Applied Physics Letters 90 (2007) 033505–33513.
[8] T. Thorsen, S.J. Maerkl, S.R. Quake, Microfluidic large-scale integration, Science 298 (2002) 580–584.
[9] I.E. Araci, S.R. Quake, Microfluidic very large scale integration (MVLSI) with integrated micromechanical valves, Lab on a Chip 12 (2012) 2803–2806.
[10] A. Douglas, A.L. Gregory, K.G. Bruce, An electrostatic microvalve for pneumatic control of microfluidic systems, Journal of Micromechanics and Microengineering 22 (2012) 025019.
[11] A.V. Desai, J.D. Tice, C.A. Apblett, P.J.A. Kenis, Design considerations for electrostatic microvalves with applications in poly(dimethylsiloxane)-based microfluidics, Lab on a Chip 12 (2012) 1078–1088.
[12] K.J. Hsia, Y. Huang, E. Menard, J.U. Park, W. Zhou, J. Rogers, J.M. Fulton, Collapse of stamps for soft lithography due to interfacial adhesion, Applied Physics Letters 86 (2005) 154106–154113.
[13] K.G. Sharp, G.S. Blackman, N.J. Glassmaker, A. Jagota, C.-Y. Hui, Effect of stamp deformation on the quality of microcontact printing: theory and experiment, Langmuir 20 (2004) 6430–6438.
[14] Z. Wu, Z. Chen, X. Du, J.M. Logan, J. Sippel, M. Nikolou, K. Kamaras, J.R. Reynolds, D.B. Tanner, A.F. Hebard, A.G. Rinzler, Transparent, conductive carbon nanotube films, Science 305 (2004) 1273–1276.
[15] Y. Zhou, L. Hu, G. Gruner, A method of printing carbon nanotube thin films, Applied Physics Letters 88 (2006) 123109–123113.
[16] A. Thangawng, R. Ruoff, M. Swartz, M. Glucksberg, An ultra-thin pdms membrane as a bio/micro–nano interface: fabrication and characterization, Biomedical Microdevices 9 (2007) 587–595.
[17] V. Studer, G. Hang, A. Pandolfi, M. Ortiz, W.F. Anderson, S.R. Quake, Scaling properties of a low-actuation pressure microfluidic valve, Journal of Applied Physics 95 (2004) 393–398.
[18] T. Bansal, M.-P. Chang, M.M. Maharbiz, A class of low voltage, elastomer-metal 'wet' actuators for use in high-density microfluidics, Lab on a Chip 7 (2007) 164–166.
[19] M.-P. Chang, M.M. Maharbiz, Electrostatically-driven elastomer components for user-reconfigurable high density microfluidics, Lab on a Chip 9 (2009) 1274–1281.
[20] B.S. Driggs, M.M. Enzelberger, S.R. Quake, Electrostatic valves for microfluidic devices, US Patent 7232109 (2002).
[21] M.A. Unger, Electrostatic/electrostrictive actuation of elastomer structures using compliant electrodes, US Patent 7075162 (2007).
[22] E. Yıldırım, M.A.S. Arıkan, H. Külah, A normally-closed electrostatic parylene microvalve for micro total analysis systems, Sensors and Actuators A: Physical 181 (2012) 81–86.
[23] E. Yıldırım, H. Külah, Analysis and characterization of an electrostatically actuated in-plane parylene microvalve, Journal of Micromechanics and Microengineering 21 (2011) 105009.
[24] D. Juncker, M., Nannini, V. Logiudice, Electrical microvalve and method of manufacturing thereof, Int. Pat. 12513381 (2007).
[25] N. Bowden, S. Brittain, A.G. Evans, J.W. Hutchinson, G.M. Whitesides, Spontaneous formation of ordered structures in thin films of metals supported on an elastomeric polymer, Nature 393 (1998) 146–149.
[26] N. Pekas, Q. Zhang, M. Nannini, D. Juncker, Wet-etching of structures with straight facets and adjustable taper into glass substrates, Lab on a Chip 10 (2010) 494–498.
[27] C. Liu, Recent developments in polymer mems, Advanced Materials 19 (2007) 3783–3790.
[28] L. Hu, D.S. Hecht, G. Grüner, Percolation in transparent and conducting carbon nanotube networks, Nano Letters 4 (2004) 2513–2517.
[29] M. Kaempgen, G.S. Duesberg, S. Roth, Transparent carbon nanotube coatings, Applied Surface Science 252 (2005) 425–429.
[30] R. Andrews, M.C. Weisenberger, Carbon nanotube polymer composites, Current Opinion in Solid State and Materials Science 8 (2004) 31–37.
[31] J.N. Coleman, U. Khan, W.J. Blau, Y.K. Gun'ko, Small but strong: a review of the mechanical properties of carbon nanotube–polymer composites, Carbon 44 (2006) 1624–1652.
[32] J. Engel, J. Chen, C. Nannan, S. Pandya, L. Chang, Multi-walled carbon nanotube filled conductive elastomers: materials and application to micro transducers, in: Proceedings of the 19th IEEE International Conference on Micro Electro Mechanical Systems, 22-26 January, Istanbul, 2006, pp. 246–249.
[33] M.P. de Boer, T.A. Michalske, Accurate method for adhesion of cantilever beams, Journal of Applied Physics 86 (1999) 817–827.
[34] E.E. Parker, W.R. Ashurst, C. Carraro, R. Maboudian, Adhesion characteristics of mems in microfluidic environments, Journal of Microelectromechanical Systems 14 (2005) 947–953.
[35] Z. Yapu, Stiction and anti-stiction in mems and nems, Acta Mechanica Sinica 19 (2003) 1–10.
[36] C. Cabuz, E.I. Cabuz, T.R. Ohnstein, J. Neus, R. Maboudian, Factors enhancing the reliability of touch-mode electrostatic actuators, Sensors and Actuators A: Physical 79 (2000) 245–250.
[37] B. Byunghoon, H. Jeahyeong, R.I. Masel, M.A. Shannon, A bidirectional electrostatic microvalve with microsecond switching performance, Journal of Microelectromechanical Systems 16 (2007) 1461–1471.
[38] M.J. Owen, P.J. Smith, Plasma treatment of polydimethylsiloxane, Journal of Adhesion Science and Technology 8 (1994) 1063–1075.
[39] S. Timoshenko, S. Woinowsky-Krieger, Theory of Plates and Shells, 2nd edition, McGraw-Hill Book Company, New York, 1959.
[40] C.H. Mastrangelo, C.H. Hsu, Mechanical stability and adhesion of microstructures under capillary forces - part ii: Experiments, Journal of Microelectromechanical Systems 2 (1993) 44–55.
[41] K. Yoshida, S. Tanaka, Y. Hagihara, S. Tomonari, M. Esashi, Normally closed electrostatic microvalve with pressure balance mechanism for portable fuel cell application, Sensors and Actuators A: Physical 157 (2010) 290–298.